TG-981
MARCH 1968
Copy No.

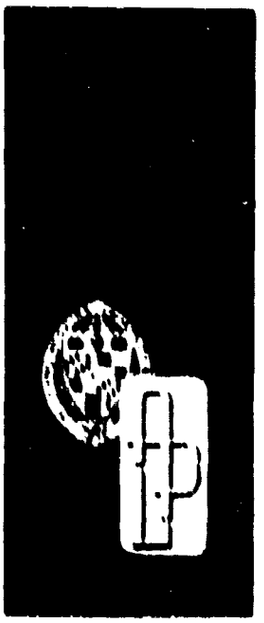

Technical Memorandum

AIR PROPERTIES AND FLOW CONDITIONS AROUND THE NOSE OF A BLUNT RADOME

by M. B. TATE

THE JOHNS HOPKINS UNIVERSITY • APPLIED PHYSICS LABORATORY

DISCLAIMER NOTICE

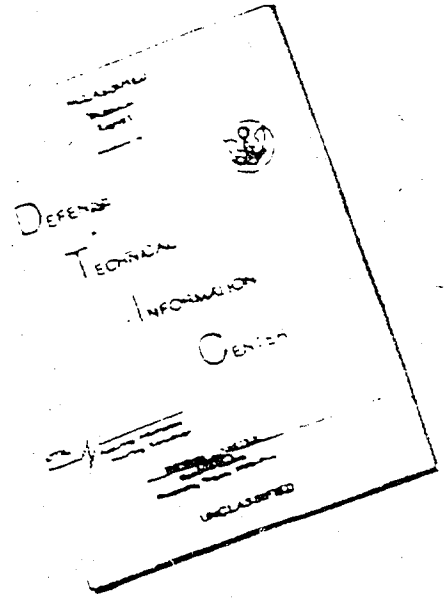

THIS DOCUMENT IS BEST QUALITY AVAILABLE. THE COPY FURNISHED TO DTIC CONTAINED A SIGNIFICANT NUMBER OF PAGES WHICH DO NOT REPRODUCE LEGIBLY.

TG-981
MARCH 1968

Technical Memorandum

AIR PROPERTIES AND FLOW CONDITIONS AROUND THE NOSE OF A BLUNT RADOME

by M. B. TATE

THE JOHNS HOPKINS UNIVERSITY • APPLIED PHYSICS LABORATORY
8621 Georgia Avenue, Silver Spring, Maryland 20910
Operating under Contract NOw 62-0604-c with the Department of the Navy

ABSTRACT

In order to correlate data obtained in tests at the Ordnance Aerophysics Laboratory on Von Karman radomes with theoretical analyses of thermal stresses in ogive radomes, the temperature and flow conditions around the nose of a blunt radome were investigated and the results are reported herein.

The blunt nose causes a detached shock wave to form with a transonic flow region developed between the wave front and the nose. Approximate solutions for the velocity components in the highly nonlinear behavior are obtained, and detachment distances compared with published experimental data. Subsonic and supersonic compressible flows are studied, and the incompressible case is shown for comparison.

Two numerical examples are given to illustrate the evaluation of initially unknown exponents and the computation of constants in the velocity equations.

TABLE OF CONTENTS

LIST OF ILLUSTRATIONS

INTRODUCTION

The OAL* aerodynamic heating tests (Reference (1)) were conducted on Von Karman radomes. Theoretical analyses have been developed for ogive radomes (Reference (2)) for the prediction of thermal stresses. Temperature-dependent material properties were investigated in Reference (3) and radome characteristics in Reference (4). Based on these investigations, it was concluded that the principal factor in expression of the different equations and correlations between test and theory is the coordinate angle (ψ), which is defined in Figure 1.

The authors of Reference (5) have pointed out that there are no theoretical solutions for flow conditions behind a detached shock wave and along the surface of a blunt body, but they do present experimental data that is plotted in Figure 2 for a sphere. The test measurements were obtained for the ratio (h_o/R_a) of the detachment distance divided by the spherical radius.

Since 1957, a great many investigations have been successfully conducted on high-speed flow problems (References (6) to (16), inclusive). Russian scientists, References (6) and (7), set up a system of integral equations that they solved numerically by extensive computer programs. These procedures were adopted and extended in the USA between 1958 and 1963, as discussed in References (8) through (12)**. In the field of physical chemistry, Lighthill (13) and Whitman (14) developed formulas for shock detachment distances based on gas ionization and dissociation phenomena. Later (1964), experimental techniques for measuring detachment distances were described in Reference (15) and numerical methods for the calculation of flow properties were again reported in 1965 (Reference (16)).

The present study grew out of the need for analyical functions in thermal-stress analysis. The investigations reviewed in the preceding paragraph lead to valuable point-to-point numerical data on flow characteristics; and the functional forms gained herein, usually by the insertion of empirical coefficients, furnish mathematical expressions that are applicable along a radome surface in terms of the radome coordinates, which govern the thermal-stress behavior.

The relationships are especially necessary at and near the radome nose where the maximum temperature occurs, and the thermal stresses tend to increase owing to

---

* Ordnance Aerophysics Laboratory, General Dynamics.
** An excellent bibliography is given in Reference (12).

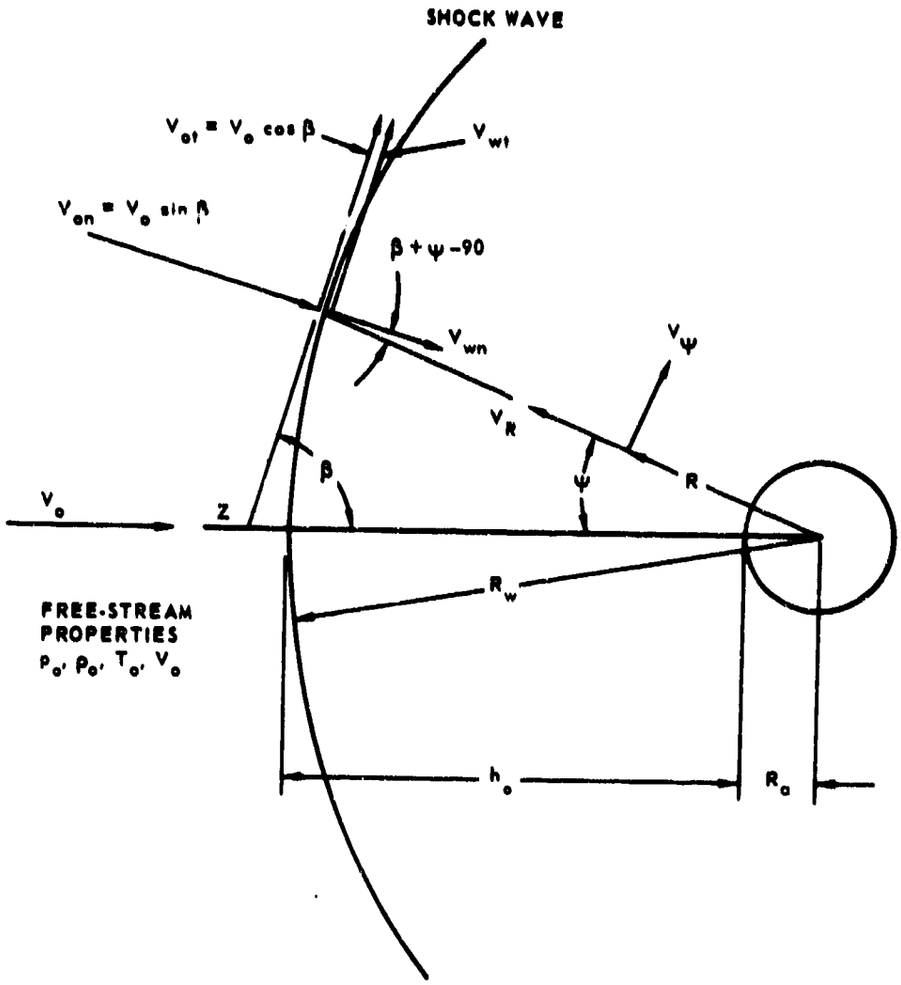

Fig. 1 VELOCITY COMPONENTS AHEAD OF AND BEHIND A DETACHED SHOCK WAVE

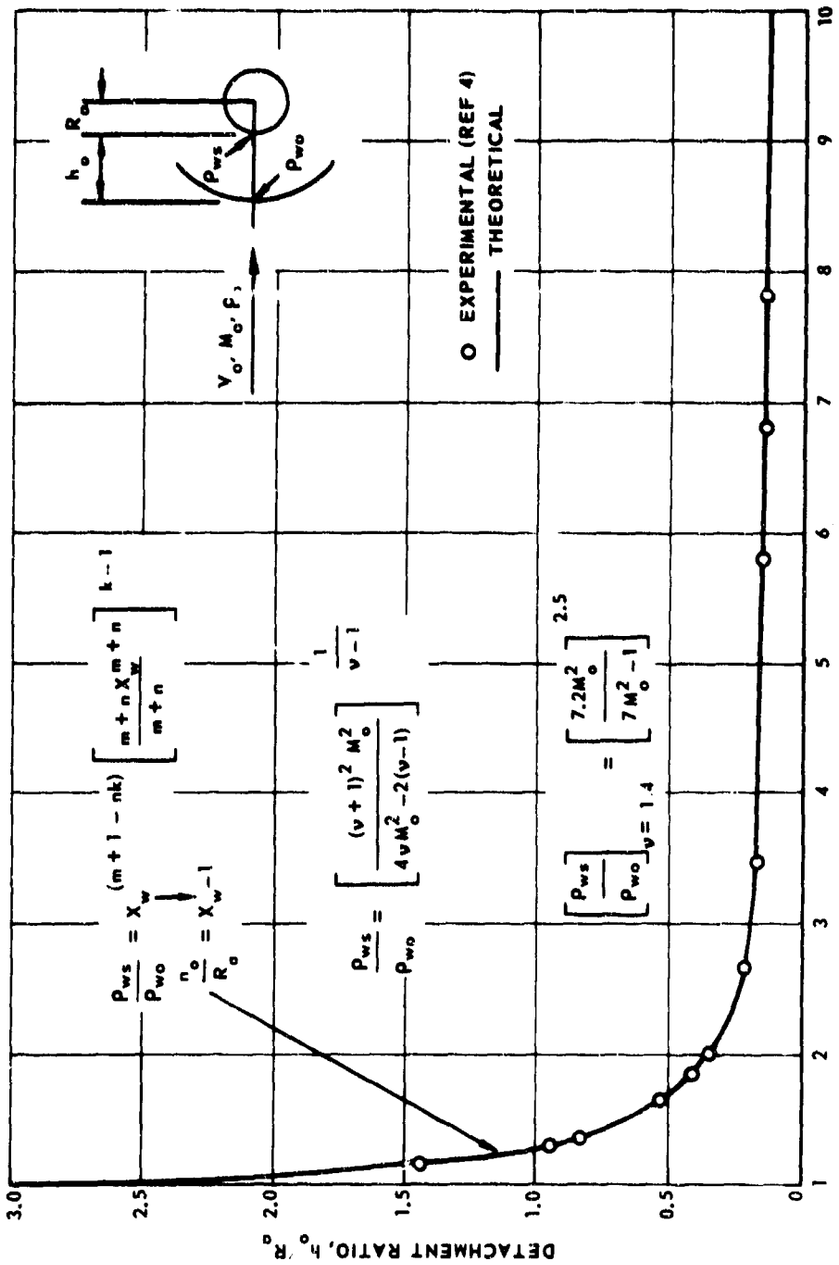

Fig. 2 SHOCK DETACHMENT RATIOS FOR A SPHERE

the small curvature radii that prevail in this region. The componental velocity equations are presented and discussed in the ensuing text, and they are derived in the appendices. Two numerical examples are worked out and the results tabulated in the final appendix.

NOMENCLATURE

The following notations are used in the text and appendices of this report:

A,B,C,D:	Constants
F:	Function
J,K:	Constants
M:	Mach number
P:	Function
R:	Radius, inches
T:	Temperature, °F or °R
U:	Function
V:	Velocity, fps
X,Y,Z:	Cartesian reference axes
a,b:	Constants
c:	Sonic speed, fps
h:	Displacement of a detached shock wave, inches
k,m,n:	Exponents
p:	Pressure, psi or psf
q:	Exponent
r:	Radius, inches
x:	Auxiliary variable ($x = R/R_a$)
α:	Angular coefficient, radians
β:	Shock wave angle, degrees
γ:	Ratio of specific heats, c_p/c_v, ($\gamma = 1.4$ for air)
λ:	Constant
ρ:	Density, scf
ψ:	Coordinate angle, degrees or radians

The following symbols appear as subscripts:

a:	Values at surface "a"
n:	Normal
o:	Free-stream values
p:	Pressure
s:	Stagnation
t:	Tangential
v:	Volume
w:	Shock-wave values
R:	In radial direction
ψ:	In ψ direction

DETACHED SHOCK-WAVE LOCATION

Approximate Formulas--The detachment distance h_o (Figure 1) is the distance along the geometric Z-axis between the shock wave and the radome nose. It is contained in X_w as

$$X_w = \frac{R_w}{R_a} = 1 + \frac{h_o}{R_a} \tag{1}$$

where R_w is the radial distance from the origin to the wave, and R_a is the radius of a spherical body. Therefore, X_w is a dimensionless ratio, and the variable ratio is

$$X = R/R_a \tag{2}$$

with R being the radial distance to any point in the flow region, and R is positioned by the coordinate angle ψ as sketched in Figure 1.

The detachment distance (h_o) is contained implicitly in the relation

$$\frac{\rho_{ws}}{\rho_{wo}} = X_w^{(m+1-nk)} \left[\frac{m + n X_w^{m+n}}{m + n} \right]^{k-1} \qquad (3)$$

wherein the exponents (k, m, n) are dependent on the free-stream Mach number (M_o), the radome dimension R_a, and the air-property ratio $\gamma = 1.4$, which is the specific-heat ratio ($\gamma = c_p/c_v$). The densities appearing in equation (3) occur at the radome-nose stagnation point (ρ_{ws}) and immediately behind the wave (ρ_{wo}) on the Z-axis. Methods for the calculation of exponents k, m, and n are described in the appendices, and the densities are computed from the well known formulas which follow.

$$\frac{\rho_{ws}}{\rho_{wo}} = \left[\frac{(\gamma+1)^2 M_o^2}{4\gamma M_o^2 - 2(\gamma-1)} \right]^{\frac{1}{\gamma-1}} \qquad (4)$$

$$\rho_{wo} = (\rho)_{\substack{R=R_w \\ \psi=o}} = \frac{\rho_o (\gamma+1) M_o^2}{2 + (\gamma-1) M_o^2} \qquad (5)$$

The densities (4) and (5) can be calculated directly when M_o is known or assigned and with $\gamma = 1.4$. Calculations involving equation (3) are normally carried out by the trial-and-error method, and the various relationships are discussed more fully in the appendices.

Experimental Data--Test data on detachment lengths are reported in Reference (5) for spheres, circular cylinders, flat plates, and flat nosed bodies of revolution. The tests were conducted by the NACA, NOL, CIT, and in Japan.* The discussions in the present report pertain to the sphere only, and the test data plotted in Figure 2 were obtained from Reference (5) p. 105.

* NACA = National Advisory Committee for Aeronautics.
NOL = U.S. Naval Ordnance Laboratory.
CIT = California Institute of Technology.

AIR VELOCITY EQUATIONS

Incompressible Flow--The equations for incompressible flow are given for purposes of comparison (Appendix A) and are:

$$V_R = -V_0 \cos\psi \left(1 - \frac{1}{X^3}\right), \qquad V_\psi = +V_0 \sin\psi \left(1 + \frac{1}{2X^3}\right) \tag{6}$$

where X is the variable ratio $X = R/R_a$, and the velocity that is tangential to the spherical surface is shown below.

$$V_a = (V_\psi)_{R = R_a} = 1.5\, V_0 \sin\psi \tag{7}$$

Subsonic Compressible Flow--The velocity components for subsonic and sonic ($M_0 \leq 1$) compressible flow are taken from Appendix B as follows:

$$V_R = -V_0 \cos\psi \left[\frac{U'}{U'_w} + A\cos^2\psi \sin\alpha(X-1)\right] \tag{8}$$

$$V_\psi = \frac{V_0 \sin\psi}{R}\left[\frac{U}{U'_w} - \frac{3AR_a\cos^2\psi}{\alpha}\left\{1 + \cos\alpha(X-1)\right\}\right] \tag{9}$$

$$X = \frac{R}{R_a}, \qquad \alpha = \frac{\pi}{X_w - 1}, \qquad A = \frac{R_a U''_w}{\alpha U'_w} \tag{10}$$

where $\sin\alpha\,(X_w-1) = 0$, $\cos\alpha\,(X_w-1) = 1$, and U is a power function of R expressed in terms of the variable X as written below.

$$U = \frac{R_a}{k}\left(\frac{X^m}{m} + \frac{1}{nX^n}\right)^k \tag{11}$$

The exponents (k, m, n) employed in the function U depend on the free-stream Mach number (M_o), the radome dimensions, and the ratio γ of the specific heats of air. Evaluations of the exponents are explained in Appendix D, and numerical values are obtained in Appendix E. From the latter appendix with $M_o = 1$, the numerical results are:

$$M_o = 1; \qquad m = 0.1; \qquad n = 1.6204; \qquad k = 12.282 \tag{12}$$

and the velocity which is tangential to the outer surface of the sphere pictured in Figure 1 is

$$V_a = (V_\psi)_{R = R_a} = V_o \sin\psi \,(1.28 - 0.4\cos^2\psi) \tag{13}$$

which can be compared with the V_a of equation (7) that was derived for the conditions of incompressible flow.

Supersonic Compressible Flow--When the free-stream flow is supersonic ($M_o > 1$), the components of velocity between the shock wave and the sphere (Figure 1) are developed in Appendix C in the form given below.

$$V_R = -V_o\cos\psi\left[\frac{KU'}{U'_w} + \frac{B\sin\alpha_1(X-1)}{\cos^2\psi} + A\cos^2\psi\,\sin\alpha(X-1)\right] \tag{14}$$

$$V_\psi = \frac{V_o\sin\psi}{R}\left[\frac{KU}{U'_w} + \frac{BR_a\cos\alpha_1(X-1)}{\alpha_1\cos^2\psi} - \frac{3AR_a\cos^2\psi}{\alpha}\left\{1 + \cos\alpha(X-1)\right\}\right] \tag{15}$$

$$X = \frac{R}{R_a}, \qquad \alpha = \frac{\pi}{X_w - 1}, \qquad \alpha_1 = \frac{\pi}{2(X_w - 1)}, \qquad A = \frac{KR_a U'_w}{\alpha U'_w} \tag{16}$$

$$B = \frac{2}{(\gamma+1)\,M_o^2}, \qquad K = \frac{\gamma-1}{\gamma+1} \tag{17}$$

The trigonometric functions at the outer boundary ($X = X_w$) become $\sin \alpha_1 (X_w - 1) = 1$, $\cos \alpha_1 (X_w - 1) = 0$, $\sin \alpha (X_w - 1) = 0$, and $\cos \alpha (X_w - 1) = -1$; and, at the inner boundary ($X = 1$), the sines vanish and the cosines equal unity. The function U is defined by equation (11).

For large values of M_o, the constant ω (equation 17) can be neglected; and numerical results from Appendix E are: (See Appendices C, D, and E)

$$M_o \geq 6; \qquad m = 0.927; \qquad n = 1.4; \qquad k = 1 \tag{18}$$

$$V_a = V_o \sin \psi \, (1.129 - 0.0114 \cos^2 \psi) \tag{19}$$

TEMPERATURE RELATIONS

Inasmuch as the present investigation was made to find suitable analytical functions for the computation of thermal stresses, the velocity functions are employed to represent temperature distributions over the radome nose. By means of the air energy equation, the surface temperatures (T_a) are expressed as

$$T_a = T_o + \frac{V_o^2 - V_a^2}{2 c_p} = T_s - \frac{V_a^2}{2 c_p} \tag{20}$$

in which $T_s = (T)_{X=1,\ \psi=o}$ is the stagnation temperature at the radome nose, and c_p is the constant-pressure specific heat of the gas. Consistent with $\gamma = 1.4$ for air, we have

$$c_p = 6{,}006 \ (\text{fps})^2/^\circ\text{R} \tag{21}$$

so equation (20) can be written

$$T_a = T_s - \frac{V_a^2}{12{,}012} \tag{22}$$

and, with equation (15), one can find V_a.

$$V_a = V_o \sin\psi \left[\frac{KU_a}{R_a U_w} + \frac{B}{\alpha_1 \cos^2\psi} - \frac{6A\cos^2\psi}{\alpha} \right] \tag{23}$$

For a specific radome, we shall let

$$\frac{KU_a}{R_a U_w} = A_o, \qquad \frac{B}{\alpha_1} = A_1, \qquad \frac{6A}{\alpha} = A_2 \tag{24}$$

and write equation (23) in the following manner.

$$V_a = V_o \sin\psi \, (A_o + A_1 \sec^2\psi - A_2 \cos^2\psi) \tag{25}$$

One of the advantages of the preceding type of equation, arising with radome noses that are only approximately spherical, is that the A_1 can be found empirically rather than by applying equations (24).

By placing equation (25) into (22), we find that T_a can be expressed as a series in $\cos\psi$; i.e.,

$$T_a = T_s - \frac{V_o^2}{2\,c_p} \sum_{n=-2}^{n=3} a_n (\cos\psi)^{2n} \tag{26}$$

where the a_n are listed in Table 1 below.

Table 1 - Series Coefficients a_n

n	a_n
-2	A_1^2
-1	$A_2(2A_o - A_1)$
0	$A_o^2 - 2A_1(A_o + A_2)$
1	$2A_2(A_1 - A_o) - A_o^2$
2	$A_2(2A_o + A_2)$
3	$-A_2^2$

In the manner just described, we can obtain integrable functions of ψ that are applicable to the theory presented in Reference (2) for radome thermal stresses. The calculations with equations (25) or (26) must in all cases be restricted to values of the coordinate angle in the range $0 \leq \psi \leq \psi_1$, where ψ_1 is the Mach angle computed from

$$\cos \psi_1 = 1/M_o \tag{27}$$

and, in general, since the approximations limit the analyses to small angles, one should probably not extend the calculations beyond about 30° even when ψ_1 exceeds this value.

DISCUSSION

The approximate solutions obtained herein have been checked in a few instances with experimental data and seem to be satisfactory for engineering calculations. However, the limits of their applicability have not been fully determined at this time, and it appears that they should not be employed much beyond $\psi = 30°$.

For calculations with angles larger than $\psi_1 = \cos^{-1}(1/M_o)$ when this angle is less than 30°, the analyst would need to omit the $\sec^2\psi$ term that occurs in equations (14), (15), (23), (25), and (26) and fit a solution of the kind represented by equations (8), (9) and exemplified by (13) and (19) to the interval $\psi_1 \leq \psi \leq 30°$.

CONCLUDING REMARKS

It is tentatively concluded that the velocity tangential to the radome nose for which analytical expressions are derived in this report, can be used to compute surface temperatures that are suitable for the prediction of thermal stresses.

Furthermore, it appears that empirical coefficients can be employed to obtain semiempirical functions in the present solutions in cases

where the radome nose is a nonspherical body of revolution, which is the situation that arises when one has to deal with the Von Karman radome.

APPENDICES

Appendix A: Incompressible Flow--The equations of fluid flow are nonlinear, and their general solution is unknown. To illustrate the procedure for obtaining approximate solutions, we shall first consider the case of incompressible flow, which also provides a limiting case for useful comparisons.

The boundary conditions (Figure 1) are:

$$(V)_{R=\infty} = V_o, \qquad (V_R)_{R=\infty} = -V_o \cos\psi, \qquad (V_\psi)_{R=\infty} = V_o \sin\psi \tag{A1}$$

$$(V_R)_{R=R_a} = 0, \qquad (V_\psi)_{R=R_a} = V(\psi) \tag{A2}$$

and for axially symmetric steady flow, the continuity equation is as follows.

$$\frac{\partial(\rho r R V_R)}{\partial R} + \frac{\partial(\rho r V_\psi)}{\partial \psi} = 0 \tag{A3}$$

In polar coordinates (R, ψ), the cross-sectional radius is $r = R\sin\psi$; and the density is nearly constant when the free-stream velocity V_o is small enough to assume that the flow is incompressible. Under these conditions, one knows that equation (A3) can be solved by employing a power function of R multiplied by a sine or cosine function of ψ. Therefore, in order to satisfy the boundary conditions (A1 and A2), one chooses

$$V_R = -V_o \cos\psi \frac{dU}{dR} = -V_o U' \cos\psi \tag{A4}$$

where $U = U(R)$ is a function of R alone. From potential theory, we have

$$\frac{\partial V_R}{\partial \psi} = \frac{\partial(R V_\psi)}{\partial R} \tag{A5}$$

which together with (A4) leads to

$$V_\psi = \frac{V_o U \sin \psi}{R} . \qquad \text{(A6)}$$

If we further select U as a power function in the form

$$U = R + (R_a/n)(R_a/R)^n = R_a(X + 1/nX^n) \qquad \text{(A7)}$$

where the variable ratio R/R_a is represented by $X = R/R_a$ and n is an undetermined exponent, the first derivative is

$$U' = (1 - 1/X^{n+1}) \qquad \text{(A8)}$$

and the boundary requirements (A1) and (A2) are fulfilled by equations (A4), (A6), (A7), and (A8).

The unknown exponent n is found by substituting the foregoing relations into the continuity equation (A3) with the constant density term cancelled from this equation, as shown below

$$\frac{\partial}{\partial R}\left[R^2 \sin\psi \cos\psi \ (1-1/X^{n+1})\right] = \frac{\partial}{\partial \psi}\left[R_a \sin^2\psi \ (X+1/nX^n)\right] \qquad \text{(A9)}$$

which tells us that n = 2. And the velocity components become

$$V_R = -V_o\cos\psi \ (1-1/X^3), \ V_\psi = +V_o\sin\psi \ (1+1/2X^3) \qquad \text{(A10)}$$

which is the classical solution for this problem. When $R = 3R_a$ and $4R_a$, the components are

$$(V_R)_{X=3} = -0.963 \ V_o\cos\psi, \qquad (V_\psi)_{X=3} = 1.019 \ V_o\sin\psi \qquad \text{(A11)}$$

$$(V_R)_{X=4} = -0.984\ V_o \cos\psi, \qquad (V_\psi)_{X=4} = +1.008\ V_o \sin\psi \tag{A12}$$

from which it is seen that the values required by (A1) are quickly approached. Along the spherical surface (Figure 1) where $R = R_a$, the velocities are

$$(V_R)_{X=1} = 0, \qquad (V_\psi)_{X=1} = V_a = +1.5\ V_o \sin\psi \tag{A13}$$

and it is observed that the tangential velocity increases from zero at the stagnation point to $V_a = 1.5\ V_o$ at each side where $\psi = 90°$. According to Reference (5), the latter velocity approximately equals the free-stream velocity V_o when $\psi = 90°$ in the high-speed compressible flow of air.

Appendix B: Subsonic Flow--In the consideration of subsonic flows that approach the sonic range ($M_o = 1$) as an upper limit, we employ a more general function U than the one given by equation (A7). It is

$$U = \frac{R_a}{k}\left(\frac{X^m}{m} + \frac{1}{nX^n}\right)^k \tag{B1}$$

in which k, m, n are undetermined exponents, and we take the density as

$$\rho = P(R)\ F(\psi). \tag{B2}$$

where P is a function of R and F is a function of ψ.

At a finite radius $R = R_w$, as yet undetermined, the boundary conditions are

$$(V)_{R=R_w} = V_o, \qquad (V_R)_{R=R_w} = -V_o \cos\psi, \qquad (V_\psi)_{R=R_w} = +V_o \sin\psi \tag{B3}$$

and along the surface of the sperical nose of the radome, the boundary requirements remain as specified by equations (A2).

The energy equation states that

$$T_s = T + \frac{V^2}{2\,c_p} = T_o + \frac{V_o^2}{2\,c_p} \tag{B4}$$

where T_s is the stagnation temperature. The preceding equation can be expressed as

$$\frac{T_s}{T} = 1 + \frac{V^2}{2\,c_p T} = 1 + \frac{(\gamma-1)M^2}{2} \tag{B5}$$

and with isentropic compression, the density can be calculated from

$$\frac{\rho}{\rho_s} = (T/T_s)^{\frac{1}{\gamma-1}} = \left[1 + \frac{(\gamma-1)M^2}{2}\right]^{\frac{1}{1-\gamma}} \tag{B6}$$

which can be expanded to obtain

$$\frac{\rho}{\rho_s} = 1 - \frac{M^2}{2} + \frac{\gamma M^4}{8} - \frac{(2\gamma-1)M^6}{48} + - \cdots \tag{B7}$$

and, since the velocity components contain sine and cosine terms, one sees that these terms will occur in expansion (B7) as $\cos^2\psi$, and higher orders with similar powers of the sine. However, since $\sin^2\psi = 1-\cos^2\psi$, we can confine the discussion to the cosine terms. For simplicity, we shall consider the first two such terms and take

$$V_R = - V_o\left[\frac{U'\cos\psi}{U_w'} + A\cos^3\psi \sin\frac{\pi(X-1)}{(X_w-1)}\right] \tag{B8}$$

$$V_\psi = + \frac{V_o \sin\psi}{R}\left[\frac{U}{U_w'} - \frac{3AR_a(X_w-1)\cos^2\psi}{\pi}\left\{1 + \frac{\cos\pi(X-1)}{(X_w-1)}\right\}\right] \tag{B9}$$

where equation (B9) is obtained from (B8) by means of (A5).

Some abbreviation is gained by letting

$$\alpha = \pi/(X_w - 1) \tag{B10}$$

and from the boundary requirements (B3) and (A2), we find with the aid of (B1), (B8), (B9), and (B10) that

$$(V_R)_{X=X_w} = -V_o \cos\psi, \qquad \frac{U_w}{R_w U'_w} = 1 \tag{B11}$$

$$(V_R)_{X=1} = 0, \qquad V_a = V_o \sin\psi \left(\frac{U_a}{R_a U'_w} - \frac{6A\cos^2\psi}{\alpha} \right) \tag{B12}$$

$$A = \frac{R_a U''_w}{\alpha U'_w} \tag{B13}$$

wherein the last expression (for the constant A) is secured by requiring the maximum radial velocity to occur at $R = R_w$ and $\psi = 0$ according to the physical condition at this point.

When V_a (equation (B12)) reduces to V_o at $\psi = 90°$, the surface boundary condition becomes

$$\frac{U_a}{R_a U'_w} = 1 \tag{B14}$$

and further relationships between the undetermined exponents are derived from the continuity equation (A3) as shown below. In order to separate the variables, we employ the following approximations:

$$\frac{V_R}{V_o} = -\cos\psi \left[\frac{U'}{U'_w} + A\cos^2\psi \sin\alpha(X-1) \right] \approx -\frac{U'\cos\psi\,(1 + a\cos^2\psi)}{U'_w\,(1+a)} \tag{B15}$$

$$\frac{V_\psi}{V_o} = \frac{\sin\psi}{R}\left[\frac{U}{U'_w} - \frac{3AR_a\cos^2\psi}{\alpha}\left\{1 + \cos\alpha(X-1)\right\}\right] \approx \frac{U\sin\psi(1 - b\cos^2\psi)}{R\,U'_w} \qquad \text{(B16)}$$

wherein a, b represent mean values of the functional ratios; i.e.,

$$a = \left[\frac{A\,U'_w \sin\alpha(X-1)}{U'}\right]_{\text{mean}} \approx \frac{\alpha A U'_w}{2R_a U'_a} \qquad \text{(B17)}$$

$$b = \left[\frac{3AR_a U'_w}{\alpha U}\left\{1 + \cos\alpha(X-1)\right\}\right]_{\text{mean}} \approx \frac{3AR_a U'_w}{\alpha U_a} \qquad \text{(B18)}$$

and with (B2), (B15), and (B16) put into (A3), there is obtained

$$\frac{\partial}{\partial R}\left[\frac{PFK^2U'\sin 2\psi\ (1 + a\cos^2\psi)}{2\ (1 + a)\ U'_w}\right] = \frac{\partial}{\partial\psi}\left[\frac{PFU\sin^2\psi\ (1 - b\cos^2\psi)}{U'_w}\right] \qquad \text{(B19)}$$

in which the variables can be separated with each group equalling a constant that is hereafter denoted by λ.

$$\lambda = \frac{1}{UP}\cdot\frac{d(PR^2U')}{dR} = \frac{2\ (1 + a)}{F\sin 2\psi\ (1 + a\cos^2\psi)}\cdot\frac{d[F\sin^2\psi(1 - b\cos^2\psi)]}{d\psi} \qquad \text{(B20)}$$

The preceding equation leads to the following two ordinary differential equations involving the undetermined coefficient λ.

$$\frac{d\ (PR^2U')}{PR^2U'} = \frac{\lambda U\,dR}{R^2U'} \qquad \text{(B21)}$$

$$\frac{d[F\sin^2\psi\ (1 - b\cos^2\psi)]}{F\sin^2\psi\ (1 - b\cos^2\psi)} = \frac{\lambda\cos\psi\ (1 + a\cos^2\psi)\,d\psi}{(1 + a)\sin\psi\ (1 - b\cos^2\psi)} \qquad \text{(B22)}$$

Integration of (B21) and (B22) produces

$$\ln\left(\frac{PR^2U'}{P_wR_w^2U_w'}\right) = \frac{\lambda}{kmn}\ln\left[\frac{(X^{m+n}-1)\,X_w^n}{(X_w^{m+n}-1)\,X^n}\right] \tag{B23}$$

$$\ln\left[\frac{F\sin^2\psi(1-b\cos^2\psi)}{F_1\sin^2\psi_1(1-b\cos^2\psi_1)}\right] = \frac{\lambda\ln(\sin\psi\csc\psi_1)}{(1-b)}$$

$$+\frac{\lambda}{2(1+a)}\left(\frac{1+a}{1-b}+\frac{a}{b}\right)\ln\left(\frac{1-b\cos^2\psi_1}{1-b\cos^2\psi}\right) \tag{B24}$$

wherein $\psi_1 > 0$. In order to have the logarithms remain finite at $X = 1$ and $\psi = 0$, we must require that

$$\lambda = kmn, \qquad \lambda = 2(1-b) \tag{B25}$$

with the first expression deriving from equation (B23) and the second from (B24). The results for P and F then are

$$P = P_w(X_w/X)^{(m+1-nk)}\left[\frac{m+nX_w^{m+n}}{m+nX^{m+n}}\right]^{k-1}, \qquad X = R/R_a \tag{B26}$$

$$F = F_1\left[\frac{1-b\cos^2\psi_1}{1-b\cos^2\psi}\right]^q \tag{B27}$$

where the exponent q is evaluated from equations (B24) and (B25).

$$q = 2 + \frac{a(1-b)}{b(1+a)} \tag{B28}$$

From equation (B2) the density equals PF, and P_w and F_1 are found from the free-stream density at $\psi = 0$, $X = X_w$.

$$\rho = PF = \rho_o \left[\frac{1 - b}{1 - b \cos^{\mu}\psi} \right]^{q} (X_w/X)^{(m+1-nk)} \left[\frac{m + nX_w^{m+n}}{m + nX^{m+n}} \right]^{k-1} \tag{B29}$$

To summarize the conditions for computing the unknowns, we find by means of (B1), (B11), and (B25) that

$$X_w^{m+n} = \frac{\lambda + m}{\lambda - n} \tag{B30}$$

and for (B29), when $X = 1$ and $\psi = 0$, the density ratio is as shown below for the stagnation-point and free-stream densities.

$$\frac{\rho_s}{\rho_o} = X_w^{(m+1-nk)} \left[\frac{m + nX_w^{m+n}}{m + n} \right]^{k-1} \tag{B31}$$

By means of (B1), (B14), (B30), and (B31), there is obtained

$$\frac{\lambda}{\lambda - n} = \frac{\rho_o X_w^{m+2}}{\rho_s} \tag{B32}$$

and one also finds from (B30) that

$$\frac{m + n X_w^{m+n}}{m + n} = \frac{\lambda}{\lambda - n} \tag{B33}$$

which can be put into equation (B31) for further simplification of the latter. The set of equations now can be listed as

$$\text{(a)}\quad \lambda = kmn$$

$$\text{(b)}\quad \lambda = 2(1-b)$$

$$\text{(c)}\quad X_w^{m+n} = \frac{\lambda + m}{\lambda - n}$$

$$\text{(d)}\quad \rho_s/\rho_o = X_w^{(m+1-nk)}\,[\lambda/(\lambda-n)]^{k-1}$$

$$\text{(e)}\quad \frac{\lambda}{\lambda-n} = \frac{\rho_o X_w^{m+2}}{\rho_s} \qquad \text{(B34)}$$

and the solution of this set of equations (B34) is taken up in Appendix D.

Appendix C: Supersonic Flow--Ahead of the blunt body in Figure 1 for supersonic flow, a detached shock wave occurs that provides a boundary surface for the definition of R_w. Air properties behind the wave front are related to the free-stream properties in the usual way through application of the continuity, momentum, and energy equations and the universal gas law. Briefly, with n denoting normal and t tangential components, these relations are:

$$\rho_o V_{on} = \rho_w V_{wn} \qquad \text{(C1)}$$

$$p_o + \rho_o V_{on}^2 = p_w + \rho_w V_{wn}^2 \qquad \text{(C2)}$$

$$V_{ot} = V_{wt} \qquad \text{(C3)}$$

$$c_p T_o + \frac{V_o^2}{2} = c_p T_w + \frac{V_w^2}{2} = c_p T_s \qquad \text{(C4)}$$

$$p = \rho R_g T \qquad \text{(C5)}$$

$$V_{on} = V_o \sin \beta, \quad V_{ot} = V_o \cos \beta \tag{C6}$$

$$c^2 = \gamma\, p/\rho = (\gamma-1)\, c_p T \tag{C7}$$

where the last equation shows the relationship for isentropic compression. And the foregoing equations lead to the following well known relations.

$$\frac{\rho_o}{\rho_w} = \frac{V_{wn}}{V_{on}} = \frac{2[1 + (\gamma-1)M_{on}^2/2]}{(\gamma+1)\, M_{on}^2} \tag{C8}$$

The boundary-value velocities can be expressed somewhat more simply if we employ the following constants.

$$B_1 = \frac{\gamma+1}{2}, \quad K_1 = \frac{\gamma-1}{2}, \qquad B = \frac{1}{B_1 M_o^2}, \qquad K = \frac{K_1}{B_1} \tag{C9}$$

Therefore by insertion of (C9) in (C8), we may write

$$\frac{V_{wn}}{V_o} = \frac{1 + K_1\, (M_o \sin \beta)^2}{B_1 M_o^2 \sin \beta} = B \csc \beta + K \sin \beta \tag{C10}$$

and, with $\gamma = 1.4$, the above constants are

$$B_1 = 6/5, \qquad K_1 = 1/5, \qquad \text{and } K = 1/6.$$

The general boundary conditions along the spherical nose surface ($R = R_a$) are

$$(V_R)_{R = R_a} = 0, \qquad (V_\psi)_{R = R_a} = V_a = V(\psi, R_a) \tag{C11}$$

and, immediately behind the shock wave ($R = R_w$), the boundary requirements are

$$(V_R)_{R=R_w} = -\left[V_{wn}\sin(\beta+\psi) + V_{wt}\cos(\beta+\psi)\right],$$

$$(V_\psi)_{R=R_w} = V_{wt}\sin(\beta+\psi) - V_{wn}\cos(\beta+\psi) \qquad (C12)$$

but conditions (C12) are intractable at the present time owing to the difficulty imposed by the variable R_w and the unknown analytical relationship between β and ψ. Some progress can be made, however, by restricting the analysis to limited ranges of the coordinate angle ψ. If we consider the case wherein the flow region has no large departure from the longitudinal axis, we can use $\beta \approx 90°-\psi$; and the simplified boundary conditions become

$$(V_R)_{R=R_w} = -V_{wn} = -V_o\,(B\sec\psi + K\cos\psi) \qquad (C13)$$

$$(V_\psi)_{R=R_w} = +V_{wt} = +V_o\sin\psi \qquad (C14)$$

For these latter requirements, one can use

$$\alpha_1 = \pi/2(X_w-1), \qquad \alpha = \pi/(X_w-1) \qquad (C15)$$

$$V_R = -V_o\cos\psi\left[\frac{KU'}{U'_w} + \frac{B\sin\alpha_1(X-1)}{\cos^2\psi} + A\cos^2\psi\sin\alpha(X-1)\right] \qquad (C16)$$

$$V_\psi = \frac{V_o\sin\psi}{R}\left[\frac{KU}{U'_w} + \frac{BR_a\cos\alpha_1(X-1)}{\alpha_1\cos^2\psi} - \frac{3AR_a\cos^2\psi}{\alpha}\left\{1+\cos\alpha(X-1)\right\}\right] \qquad (C17)$$

where U is the power function of R given by equation (B1), and the density will again be represented by PF as shown in (B2). Again, as in Appendix B, we shall use mean values of the functional ratios in order to integrate the continuity equation (A3), and we shall find A in the same manner as described below equation (B13). Hence,

$$V_R \approx - \frac{V_o KU' \cos \psi}{U_w'} \quad (1 + a_1 \sec^2\psi + a \cos^2\psi) \tag{C18}$$

$$V_\psi \approx \frac{V_o KU \sin \psi}{R\, U_w'} \quad (1 + b_1 \sec^2\psi - b \cos^2\psi) \tag{C19}$$

$$A = \frac{KR_a U_w''}{\alpha U_w'} \tag{C20}$$

$$a_1 = \left[\frac{BU_w' \sin \alpha_1 (X-1)}{KU'}\right]_{mean} \approx \frac{B}{2K}\left(1 + \frac{\alpha_1 U_w'}{R_a U_a''}\right) \tag{C21}$$

$$a = \left[\frac{AU_w' \sin \alpha(X-1)}{KU'}\right]_{mean} \approx \frac{\alpha A U_w}{2 KR_a U_a''} \tag{C22}$$

$$b_1 = \left[\frac{BU_w' R_a \cos \alpha_1 (X-1)}{\alpha_1 KU}\right]_{mean} \approx \frac{BR_a U_w'}{2\alpha_1 KU_a} \tag{C23}$$

$$b = \left[\frac{3AR_a U_w'}{\alpha\, KU}\left\{1 + \cos \alpha(X-1)\right\}\right]_{mean} \approx \frac{3AR_a U_w'}{\alpha\, KU_a} \tag{C24}$$

Integration of the continuity equation is completed by the method explained previously in Appendix B, and we learn that

$$\lambda = kmn, \qquad \lambda = \frac{2(1 + b_1 - b)}{1 + a_1 + a} \tag{C25}$$

$$\rho = \rho_{wo} \cos^2\psi \left[\frac{C_1 + 1}{C_1 + \cos^2\psi}\right]^{q_1} \left[\frac{C_2 - 1}{C_2 - \cos^2\psi}\right]^{q_2} \left[\frac{m + nX_w^{m+n}}{m + nX^{m+n}}\right]^{k-1} (X_w/X)^{(m+1-nk)} \tag{C26}$$

$$\rho_{wo} = (\rho)_{\substack{X=X_w \\ \psi=o}} = \frac{\rho_o B_1 M_o^2}{1 + K_1 M_o^2} = \frac{\rho_o(\gamma+1)M_o^2}{2 + (\gamma-1)M_o^2} \tag{C27}$$

$$\rho_{ws} = (\rho)_{\substack{X=1 \\ \psi=o}} = \rho_{wo}\left[\frac{(B_1 M_o)^2}{\gamma M_o^2 - K_1}\right]^{\frac{1}{\gamma-1}} \tag{C28}$$

where B_1, K_1 are defined by equations (C9) and C_1, C_2, q_1, and q_2 are given below.

$$C_1 = -\frac{1}{2b} + \sqrt{\frac{1}{4b^2} + \frac{b_1}{b}}\,, \quad C_2 = \frac{1}{2b} + \sqrt{\frac{1}{4b^2} + \frac{b_1}{b}} \tag{C29}$$

$$q_1 = 2 - \frac{1 + C_1}{C_1 + C_2} - \frac{\lambda}{2b}\left[\frac{1 + a(1-C_1)}{C_1 + C_2}\right], \quad q_2 = 2 + \frac{1 - C_2}{C_1 + C_2} + \frac{\lambda}{2b}\left[\frac{1 + a(1+C_2)}{C_1 + C_2}\right] \tag{C30}$$

When the foregoing results are summarized for evaluation of the unknown exponents, we obtain a set of equations that are similar to (B36).

$$\text{(a)}\quad \lambda = kmn$$

$$\text{(b)}\quad \lambda = \frac{2(1 + b_1 - b)}{1 + a_1 + a}$$

$$\text{(c)}\quad X_w^{m+n} = \frac{\lambda + mK}{\lambda - nK} = \frac{\lambda_1 + m}{\lambda_1 - n}$$

$$\text{(d)}\quad \rho_{ws}/\rho_{wo} = X_w^{(m+1-nk)}\left[\lambda_1/(\lambda_1 - n)\right]^{k-1}$$

$$\text{(e)}\quad \frac{\lambda_1}{\lambda_1 - n} = \frac{\rho_{wo} B_1 \alpha_1 X_w^{m+2}}{\rho_{ws}(B_1\alpha_1 - 1)} \tag{C31}$$

The above set differs from the previous one primarily in the use of $\lambda_1 = \lambda/K$ (where $\lambda_1 = 6\lambda$ when $\gamma = 1.4$), the density ratio, and the additional terms in

equation (e). The density ratio is calculated with equation (C28), which, when $\gamma = 1.4$, gives us

$$\frac{\rho_{ws}}{\rho_{wo}} = \left[\frac{36M_o^2}{5(7M_o^2 - 1)} \right]^{\frac{5}{2}} \tag{C32}$$

and ρ_{wo} can be computed with equation (C27) when required. Further discussion of the solution of set (C31) is presented in the next appendix.

Appendix D: Solution of Equations--Inspection of the equation set (B36) indicates that two solutions are $m = n = 0$ and $n = -m$. These two solutions are trivial, however, and we must look beyond them to find a usable function U (equation B1). In doing so, one can regard X_w as a known quantity based on the experimental data reported in Reference (5) and plotted in Figure 2. The first solution then obtained proceeds as follows: If we use the mean value of equation (B18) together with (B13) for A, we arrive at

$$A = \frac{(\lambda+m)(\lambda-n)}{\alpha\lambda X_w} \tag{D1}$$

$$b = \frac{3A\lambda\rho_s}{\alpha\rho_o(\lambda-n)X_w^{m+2}} = \frac{3\rho_s(\lambda+m)}{\rho_o\,\alpha^2 X_w^{m+3}} \tag{D2}$$

and the known density ratio can be replaced by an exponent (m_1) of X_w as defined by equation (D3) immediately below.

$$m_1 = 2 - \frac{\ell n\,(\rho_s/\rho_o)}{\ell n\,X_w} \tag{D3}$$

In this way, we have the relation

$$\rho_o\,X_w^2/\rho_s = X_w^{m_1} \tag{D4}$$

and the equations (B36) can be written to furnish the following set wherein we let $\alpha^2\,X_w/6$ equal the known constant C.

$$\text{(a)}\quad \lambda = kmn, \quad C = \alpha^2 X_w/6$$

$$\text{(b)}\quad \lambda = 2(1-b) = 2 - \frac{(\lambda+m)(\lambda-n)}{C\lambda}$$

$$\text{(c)}\quad X_w^{m+n} = \frac{\lambda + m}{\lambda - n}$$

$$\text{(d)}\quad 1 = X_w^{(m+m_1-1-nk)} \left[\frac{\lambda}{\lambda-n}\right]^{k-1}$$

$$\text{(e)}\quad \frac{\lambda}{\lambda-n} = X_w^{m+m_1} \qquad \text{(D5)}$$

On putting (D5-e) into (D5-d), we obtain

$$k = \frac{1}{m + m_1 - n} \qquad \text{(D6)}$$

and from (a) and (b), one finds

$$\frac{1}{k} = \lambda(1+C) + m - n - 2C \qquad \text{(D7)}$$

which leads to a calculable value of λ when (D6) and (D7) are solved together.

$$\lambda = 2 + \frac{m_1 - 2}{1 + C} \qquad \text{(D8)}$$

The coefficient λ is less than 2 (since m_1 is smaller then 2) as computed from the preceding expression. After computing the above coefficient, n and k are expressed in terms of m by means of (D5-a) and D6).

$$n = \frac{\lambda\,(m + m_1)}{\lambda + m}, \qquad k = \frac{\lambda + m}{m(m + m_1)} \qquad \text{(D9)}$$

By using (D9) to replace n in (D5-e), we find

$$(\lambda - m_1)\, X_w^{m_1} = \frac{\lambda + m}{X_w^{m}} \qquad \text{(D10)}$$

and m can be calculated from (D10) by successive trials, because all quantities but m are known in this relationship. Following the numerical evaluation of m from (D10), n and k are computed with equations (D9). These values of the exponents (k, m, n) furnish sufficient information for determination of the power function U of equation (B1). The solution, however, is approximate, because (D5-c) can be rearranged to give

$$(\lambda - n) X_w^{n} = \frac{(\lambda + m)}{X_w^{m}} \qquad \text{(D11)}$$

and, by comparing (D10) and (D11), one observes that the latter is satisfied only by $n = m_1$, which fails to satisfy all of the other equations in set (D5). The approximation thus formed meets all of the boundary requirements in Appendix B with the exception of (B14), which becomes greater than unity, lying between 1 and about 1.5. This result may, nevertheless, be acceptable in many cases, because it appears likely that (B14) is too severe. We are unable to answer this question conclusively, however, since the experimental data are insufficient for definition of the correct relation.

It is necessary to consider, also, that perhaps all of the boundary conditions be relaxed to some extent as indicated by the solution in Appendix A for incompressible flow. This solution shows that the air properties differ from the free-stream values for all finite values of X_w. Employing this behavior as a guide, one can reduce requirement (B11) by a reasonable percentage, such as is exemplified by equations (A11) and (A12).

If we say that (B11) is J-percent of unity (for example, one might use J = 0.9 for a ten percent reduction), equations (D5) become

$$\text{(a)} \quad \lambda = kmn, \qquad \lambda_2 = J\lambda$$

$$\text{(b)} \quad \lambda = 2(1-b) = 2 - \frac{1}{C}\left[\frac{(\lambda_2 + m)(\lambda_2 - n)}{\lambda_2} + \frac{1-J}{J}\right]$$

$$(c)\quad X_w^{m+n} = \frac{\lambda_2 + m}{\lambda_2 - n}$$

$$(d)\quad \rho_s/\rho_o = X_w^{(m+1-nk)} \left[\lambda_2/(\lambda_2 - n)\right]^{k-1}$$

$$(e)\quad \frac{\lambda_2}{\lambda_2 - n} = X_w^{m+m_2} \qquad \text{(D12)}$$

where, in equation (D12-e), m_2 depends on the choice of J as defined by the next equation (in which m_1 is given by (D3)).

$$m_2 = m_1 + \frac{\ell n\ J}{\ell n\ X_w} \qquad \text{(D13)}$$

Upon solving the set of equations (D12), one finds that λ is no longer independent of m and n as was the case with set (D5) where the result is given by (D8). Instead, we proceed as follows: With D given by

$$D = 1 + \frac{\ell n\ J}{\ell n\ X_w} \qquad \text{(D14)}$$

we find from (D12-d) and (D12-e) that

$$k = D/(m + m_2 - n) \qquad \text{(D15)}$$

and by means of (a), (e), and (D15), n is obtained as a function of m.

$$n = m_2 + m\left[1 - (1 - 1/X_w^{m+m_2})JD\right] \qquad \text{(D16)}$$

By substituting (D12-e) into (D12-c), we find

$$X_w^{m-m_2} = 1 + \frac{m}{n}\left[1 - \frac{1}{X_w^{m+m_2}}\right] \qquad \text{(D17)}$$

which together with (D16) is solved by successive trials to obtain m. With the value of m thus found, n is calculated from (D16) and k from (D15). And these three exponents furnish sufficient information for the definition of U.

Similarly, the equation set (C31) can be evaluated by taking (C31-e) in the form

$$\frac{\lambda_1}{\lambda_1 - n} = X_w^{m+m_3} \tag{D18}$$

where m_3 is computed from

$$m_3 = 2 - \frac{\ell n(\rho_{w3}/\rho_{w0}) + \ell n(1 - 1/B_1\alpha_1)}{\ell n\, X_w} \tag{D19}$$

and the expression for k that is similar to equation (D15) is

$$k = D_1/(m + m_3 - n) \tag{D20}$$

and the n-function of m, similar to (D16), becomes

$$n = m_3 + n\left[1 - (1 - 1/X_w^{m+m_3})D_1/K\right] \tag{D21}$$

in which the term D_1 is calculated from the next expression.

$$D_1 = 1 - \frac{\ell n\,(1 - 1/B_1\alpha_1)}{\ell n\, X_w} \tag{D22}$$

Using the trial-and-error method, we then calculate m for the following relationship in conjunction with equation (D21).

$$X_w^{n-m_3} = 1 + \frac{m}{n}\left[1 - \frac{1}{X_w^{m+m_3}}\right] \tag{D23}$$

It is observed that the preceding relation is analogous to equation (D17); and after m is computed, n and k are determined by means of equations (D21) and (D20), respectively.

When it is desired to employ the reduction coefficient J, the exponents (m, n, and k) are computed from the following sequence of equations.

$$n = m_s + m\left[1 - (1 - 1/X_w^{m+m_s})JD_s/K\right] \tag{D24}$$

$$X_w^{n-m_s} = 1 + \frac{m}{n}\left[1 - \frac{1}{X_w^{m+m_s}}\right] \tag{D25}$$

$$k = D_s/(m + m_s - n) \tag{D26}$$

Exponent m is calculated by trial and error from equations (D25) and (D24) followed by the evaluation of k from (D26). The terms m_s and D_s are obtained from

$$m_s = m_1 + \frac{\ln J}{\ln X_w} \tag{D27}$$

$$D_s = D_1 + \frac{\ln J}{\ln X_w} \tag{D28}$$

where m_1 and D_1 are given by equations (D19) and (D22), respectively.

Appendix E: Numerical Examples--If we consider the case of $M_0 = 1$ and take $X_w = 4$ with the solution represented by equations (D21) to (D17), inclusive, and J = 0.9, the initially calculable terms are:

$$\rho_s/\rho_0 = 1.577 \text{ (Eq. C32)}, \quad m_1 = 1.671,470 \text{ (Eq. D3)}$$

$$m_s = 1.595,605 \text{ (Eq. D13)}, \quad D = 0.924,135 \text{ (Eq. D14)}$$

$$n = 1.595,605 + m\left[1 - 0.831,722\ (1-0.109,514 \times 4^{-m})\right] \text{(Eq. D16)}$$

$$4^{n-m_s} = 1 + \frac{m}{n}\left[1 - (0.109,514)/4^m\right] \text{(Eq. D17)}$$

$$k = \frac{0.924,135}{m + m_0 - n} \qquad \text{(Eq. D15)}.$$

Use of the trial-and-error process furnishes approximate fulfillment of equations (D16) and (D17) with m = 0.1; and from (D16) and (D15), n and k are computed and summarized below with m.

$$m = 0.1; \quad n = 1.6204; \quad k = 12.282 \qquad \text{(E1)}$$

The power function (B1) with exponents (E1) is shown below (wherein $X = R/R_a$).

$$U = \frac{R_a}{12.282}\left[10\,X^{0.1} + \frac{0.617,132}{X^{1.6204}}\right]^{12.282} \qquad \text{(E2)}$$

The first and second derivatives with respect to R become

$$U' = \left[10\,X^{0.1} + \frac{0.167,132}{X^{1.6204}}\right]^{11.282}\left(\frac{1}{X^{0.9}} - \frac{1}{X^{2.6204}}\right) \qquad \text{(E3)}$$

$$R_a U'' = 11.282\left[10\,X^{0.1} + \frac{0.617,132}{X^{1.6204}}\right]^{10.282}\left(\frac{1}{X^{0.9}} - \frac{1}{X^{2.6204}}\right)^2$$

$$+ \left[10\,X^{0.1} + \frac{0.617,132}{X^{1.6204}}\right]^{11.282}\left(\frac{2.6204}{X^{3.6204}} - \frac{0.9}{X^{1.9}}\right) \qquad \text{(E4)}$$

and from equations (E2, E3, and 4), the following numerical results were computed.

$$U_a/R_a = 3.255,587 \times 10^{11}; \qquad U_w/R_a = 9.171,341 \times 10^{11} \qquad \text{(E5)}$$

$$U_a' = 0 \qquad U_w' = 2.542,788 \times 10^{11} \qquad \text{(E6)}$$

$$R_a U_a'' = 6.479,189 \times 10^{11}; \qquad R_a U_w'' = 1.861,719 \times 10^{10} \tag{E7}$$

The numerical ratios that occur in the velocity components as calculated with equations (E5, E6, E7) and A and α are:

$$\frac{U_a}{R_a U_w'} = 1.280,322; \qquad \frac{U_w}{R_w U_w'} = 0.901,701 \tag{E8}$$

$$\alpha = \frac{\pi}{X_w - 1} = 1.0472; \qquad A = \frac{R_a U_w''}{\alpha U_w'} = 0.069,916 \tag{E9}$$

$$\frac{R_a U_a''}{U_w'} = 2.548,065; \qquad \frac{R_a U_w''}{U_w'} = 0.073,216 \tag{E10}$$

and the velocity components follow,

$$V_R = -V_o \cos\psi \left[\frac{U'}{U_w'} + (0.070) \cos^2\psi \sin\alpha(X-1) \right] \tag{E11}$$

$$V_\psi = + \frac{V_o \sin\psi}{R} \left[\frac{U}{U_w'} - (0.200) R_a \cos^2\psi \left\{ 1 + \cos\alpha(X-1) \right\} \right] \tag{E12}$$

At the outer boundary where $X_w = 4$, it is found from the preceding relations that the components are

$$(V_R)_{X_w = 4} = - V_o \cos\psi, \qquad (V_\psi)_{X_w = 4} = 0.902\, V_o \sin\psi \tag{E13}$$

and at the inner boundary along the surface of the spherical nose where X = 1, the components are as follows:

$$(V_R)_{X=1} = 0, \qquad (V_\psi)_{X=1} = V_a = V_o \sin\psi\,(1.280 - 0.4\cos^2\psi) \tag{E14}$$

The results indicate that V_a increases from zero at $\psi = 0$ to $V_a = 1.28\ V_o$ at $\psi = 90°$ with the variation tabulated in the immediately following Table 2.

Table 2 - Variation of Velocity Tangential to Spherical Nose for $M_o = 1$.

ψ (Deg.)	$\sin\psi$	$\cos\psi$	$\frac{V_a \csc\psi}{V_o}$	V_a/V_o (compressible)	V_a/V_o (incompressible)
0	0	1	0.88	0	0
30	0.5	0.866	0.98	0.490	0.750
45	0.707	0.707	1.08	0.764	1.061
60	0.866	0.5	1.18	1.022	1.299
90	1	0	1.28	1.280	1.5

If one next considers the case for large Mach numbers (say $M_o \to \infty$), the value of $X_w = 1.143$ is taken from the data in Figure 2 and $\rho_{ws}/\rho_{wo} = 1.073$ computed with equation (C32). Since the following ratio is small; i.e.,

$$(1/\alpha_1 B_1)_{M_o>6} = 5/21\pi = 0.0758 \tag{E15}$$

and will be neglected, we shall let $k = 1$ and calculate m and n from equations (C31-a, c, and d). We find that

$$n = m + 1 - \frac{\ln(1.073)}{\ln(1.143)} = m + 0.472{,}659 \tag{E16}$$

$$(1.143)^{m+n} = \frac{m(6n+1)}{n(6m-1)} \tag{E17}$$

where (E16) and (E17) are solved by successive trials to obtain m = 0.927 and n = 1.3997. The power function of R (equation B1) wherein $X = R/R_a$ is then

$$U = R_a\left(\frac{X^{0.927}}{0.927} + \frac{0.714,286}{X^{1.4}} \right) \tag{E18}$$

and the first and second derivatives are found to be

$$U' = \frac{1}{X^{0.073}} - \frac{1}{X^{2.4}} \tag{E19}$$

$$R_a U'' = \frac{2.4}{X^{3.4}} - \frac{0.073}{X^{1.073}} \tag{E20}$$

by means of which the results shown below were calculated.

$$U_a = 1.793,035R_a, \qquad U_w = 1.813,667R_a \tag{E21}$$

$$U_a' = 0 \qquad U_w' = 0.264,660 \tag{E22}$$

$$R_a U_a'' = 2.327, \qquad R_a U_w'' = 1.461 \tag{E23}$$

The ratios that appear in the expressions for the components of velocity were also evaluated; e.g.,

$$\frac{K U_a}{R_a U_w'} = 1.129; \quad \frac{K U_w}{R_w U_w'} = 0.9994 \tag{E24}$$

$$A = \frac{K R_a U_w''}{\alpha U_w'} = 0.041,837 \tag{E25}$$

and the velocity components are written as follows.

$$V_R = - V_o \cos \psi \left[\frac{U'}{1.588} + (0.0418) \cos^2 \psi \sin 7\pi(X-1) \right] \qquad \text{(E26)}$$

$$V_\psi = \frac{V_o \sin \psi}{R} \left[\frac{U}{1.588} - (0.00571) R_a \cos^2 \psi \left\{ 1 + \cos 7\pi(X-1) \right\} \right] \qquad \text{(E27)}$$

$$(V_\psi)_{R=R_a} = V_a = V_o \sin \psi \, (1.129 - 0.0114 \cos^2 \psi) \qquad \text{(E28)}$$

The variation of V_a along the surface of the spherical nose shown in Figure 1 is tabulated below in Table 3.

Table 3 - Variation of Velocity Tangential to Spherical Nose for $M_o > 6$

ψ (Deg.)	sin ψ	cos ψ	$\frac{V_a \csc \psi}{V_o}$	V_a/V_o (compressible)	V_a/V_o (incompressible)
0	0	1	1.118	0	0
30	0.5	0.866	1.120	0.560	0.750
45	0.707	0.707	1.123	0.794	1.061
60	0.866	0.5	1.126	0.975	1.299
90	1	0	1.129	1.129	1.5

REFERENCES

(1) Maytubby, D. A., "Final Test Results from the Standard Missile Type I (ER) and the Medium Range TYPHON Wind Tunnel Test Program for the Radome Assemblies" (U) (Confidential), TM-6-332-298, GD/Pomona, 1965.

(2) Tate, M. B., "Large Axisymmetric Thermal Bending Stresses in Ogival Radomes with Heat Variant Material Properties" (Unclassified), APL/BBE EM-3995, 1965.

(3) Tate, M. B., "Pyroceram 9606 Test Data for Radome Thermal Stress Analysis" (Unclassified), APL/BBE EM-3999, 1965.

(4) Tate, M. B., "Curvature Radii of Von Karman Radomes for Thermal Stress Calculations" (U) (Confidential), APL/BBE EM-4000, 1965.

(5) Liepmann, H. W. and Roshko, A., "Elements of Gas Dynamics," 2d ed, Wiley, New York, 1957.

(6) Dorodnitsyn, A. A., "Method of the Integral Relations for the Numerical Solution of Partial Differential Equations" (Unclassified), Institute of Exact Mechanics and Computing Techniques, Akademie Wauk, USSR, 1968.

(7) Belotcerkovskii, O. M., "Flow with Detached Shock Wave about a Symmetric Profile" (Unclassifed), Prickladnaia Mathematika and Mekanika, USSR, 1958.

(8) Hayes, W. O. and Probstein, R. F., "Hypersonic Flow Theory" (Unclassified), Academic Press, New York, 1959.

(9) Vaglio-Laurin, R. and Ferri, A., "Theoretical Investigation of the Flow about Blunt-Nosed Bodies in Supersonic Flight," J. Aero/Space Sci., Vol. 25, No. 12, 1958, pp. 761-770.

(10) Vaglio-Laurin, R., "Turbulent Heat Transfer of Blunt-Nosed Bodies in Two-Dimensional and General Three-Dimensional Hypersonic Flow," J. Aero/Space Sci., Vol. 27, No. 1, 1960, pp. 27-36.

(11) Vaglio-Laurin, R., "On the PLK Method and the Supersonic Blunt-Body Problem," J. Aero/Space Sci., Vol. 29, No. 29, 1962, p. 185.

(12) Ferri, A. and Vaglio-Laurin, R., "External Hypersonic Flows, A Review of Current Problems and Methods of Analysis Including Physicochemical Effects," Aerospace Eng., Vol. 22, No. 1, 1963, p. 23.

(13) Lighthill, M. J., "Dynamics of a Dissociating Gas," J. Fluid Mech., Vol. 2, No. 1, 1958, p. 1.

(14) Whitman, G. B., "A Note on the Stand-Off Distance of the Shock in High Speed Flow Past a Circular Cylinder," Communs. Pure and Appl. Math., Vol. X, No. 4, 1957, p. 531.

(15) Lobb, R. K., "Experimental Measurement of Shock Detachment Distances on Spheres Fired in Air," The High Temperature Aspects of Hypersonic Flow, Chap. 26, The Pergamon Press, New York, 1964.

(16) Lomax, H. and Inovye, M., "Numerical Analysis of Flow Properties about Blunt Bodies Moving at Supersonic Speeds" (Unclassified), NASA TR-R-204, National Aeronautics and Space Administration, ARC, Moffett Field, California, 1965.

UNCLASSIFIED
Security Classification

DOCUMENT CONTROL DATA - R & D

Security classification of title, body of abstract and indexing annotation must be entered when the overall report is classified)

1. ORIGINATING ACTIVITY (Corporate author) The Johns Hopkins University, Applied Physics Lab. 8621 Georgia Avenue Silver Spring, Maryland	2a. REPORT SECURITY CLASSIFICATION Unclassified 2b. GROUP n. a.

3. REPORT TITLE

Air Properties and Flow Conditions Around the Nose of a Blunt Radome

4. DESCRIPTIVE NOTES (Type of report and inclusive dates)

Technical Memorandum

5. AUTHOR(S) (First name, middle initial, last name)

Manford B. Tate

6. REPORT DATE	7a. TOTAL NO. OF PAGES	7b. NO. OF REFS
	38	16

8a. CONTRACT OR GRANT NO.	9a. ORIGINATOR'S REPORT NUMBER(S)
NOw 62-0604-c b. PROJECT NO.	TG-981
c. d.	9b. OTHER REPORT NO(S) (Any other numbers that may be assigned this report) n. a.

10. DISTRIBUTION STATEMENT

This document has been approved for public release and sale; its distribution is unlimited.

11. SUPPLEMENTARY NOTES	12. SPONSORING MILITARY ACTIVITY
	NAVORDSYSCOM

13. ABSTRACT

In order to correlate data obtained in OAL (Ordnance Aerophysics Laboratory, Daingerfield Division, General Dynamics/Pomona, Daingerfield, Texas) tests on Von Karman radomes with theoretical analyses of thermal stresses in ogive radomes, the temperature and flow conditions around the nose of a blunt radome were investigated, and the results are reported herein. The blunt nose causes a detached shock wave to form with a transonic flow region developed between the wave front and the nose. Approximate solutions for the velocity components in the highly nonlinear behavior are obtained, and detachme ' distances compared with published experimental data. Subsonic and supersonic compressible flows are studied, and the incompressible case is shown for comparison. Two numerical examples are given to illustrate the evaluation of initially unknown exponents and the computation of constants in the velocity equations.

DD FORM 1 NOV 1473

UNCLASSIFIED
Security Classification

14. KEY WORDS

Blunt radome air flow

Detached shock wave

Blunt radome temperature relations